*Article*

# Theoretical evaluation of novel Thermolysin inhibitors from *Bacillus thermoproteolyticus* as possible antibacterial agents.

**Emilio Lamazares** [1], **Desmond MacLeod-Carey** [2,] **Fernando P. Miranda** [3] **and Karel Mena-Ulecia** [4,5,*]

[1] Universidad de Concepción, Biotechnology and Biopharmaceutical Laboratory, Pathophysiology Department; School of Biological Sciences, Victor Lamas 1290, P.O. Box 160-C, Concepción, Chile; elamazares@udec.cl

[2] Universidad Autónoma de Chile, Facultad de Ingeniería, Instituto de Ciencias Químicas Aplicadas, Inorganic Chemistry and Molecular Materials Center, El Llano Subercaseaux 2801, San Miguel, Santiago, Chile.; desmond.macleod@uautonoma.cl

[3] Instituto de Fisiología, Facultad de Medicina, Universidad Austral de Chile.; fmiranda959@gmail.com

[4] Departamento de Ciencias Biológicas y Químicas, Facultad de Recursos Naturales. Universidad Católica de Temuco. Ave. Rudecindo Ortega 02950, Temuco, Chile; kmena@uct.cl

[5] Núcleo de Investigación en Bioproductos y Materiales Avanzados (BIOMA), Facultad de Ingeniería, Universidad Católica de Temuco. Ave. Rudecindo Ortega 02950, Temuco, Chile.; kmena@uct.cl

* Correspondence: kmena@uct.cl; Tel.: +56-9-6603-2531 (C.L.)

**Abstract:** The search for new antibacterial agents that could decrease bacterial resistance is a subject that is continuously developing. The Gram-negative and Gram-positive bacteria have a metalloproteins group belonging to the M4 family. That is the main virulence factor of these bacteria. In this work, we have used a computational protocol based on the comprehensive analysis of the results of docking, molecular dynamics simulation, MM-PBSA, ligand efficiency, and ADME-Tox properties of ligand designed *in silico* in the previous manuscript using the Thermolysin from *Bacillus thermoproteolyticus*, a metalloprotein of the M4 family as a target. The principal results obtained were the designed ligands were adequately oriented in the thermolysin active center. The Lig783, Lig2177, and Lig3444 compounds were those with better dynamic behavior, however, when analyzing the results extracted from the ADME-Tox properties, only Lig783 was the best antibacterial agent candidate.

**Keywords:** Thermolysin; Antibacterial agents; Docking; Molecular dynamics; MM-PBSA, ADME-Tox.

## 1. Introduction

The increase in bacterial diseases around the world has been relevant in recent years[1]. It is proposed that for this year 2020, more than 117 conditions of bacterial origin will be described worldwide. Because of the increase in bacterial infections, the World Health Organization (WHO) assigned the highest priority to the research and development of antibacterial drugs to combat Gram-positive and Gram-negative bacteria[2].

Bacteria of the *Vibrio*, *Legionella*, *Clostridium*, *Listeria*, *Staphylococcus*, and *Pseudomonas* genus are critical factors of various diseases such as cholera[3,4], ulcerative gastritis[5], and gastric carcinoma[6], affecting millions of people around the world. These bacteria have a significant group

of proteins in common that are crucial factors in the several diseases pathogenesis [7]. This group of proteins is called the M4 Family[8].

An M4 family is an essential metalloproteins group that has close similarities between them[9]. This group of proteins is commonly called the Thermolysin-Like-Proteinase (TLPsa) family[9]. This name is because of the high similarity present with thermolysin since they have a consensus sequence (HExxH)[7], which is part of the catalytic domain together with $Zn^{2+}$. Therefore, the search for effective inhibitors of M4 family proteins, including thermolysin, is one of the novel strategies in the design of third and fourth generation antibiotics[10].

The Thermolysin is secreted by *Bacillus thermoproteolyticus*, and it is considered a metalloproteinase containing $Zn^{2+}$ in its active center, which is essential in the catalytic activity of this enzyme[7]. This protein was one of the first metalloproteins to be isolated. Its crystallographic structure was resolved; that´s why it is widely used as a model in studying several diseases[11,12]. Our group designed new Thermolysin inhibitors in previous work using a combination of two methods, QSARIN, and Virtual screening, as possible antihypertensive drugs[11]. Six compounds were obtained from this study (Figure 10), which must be evaluated as possible antibacterial agents. We offer a computational biochemistry protocol based on docking, molecular dynamics simulation, MM-PBSA, ADME-Tox, and ligand efficiency methodologies in the comprehensive evaluation of these molecules as possible to meet this goal antibacterial agents, whose results are shown below.

## 2. Results and Discussion

### 2.1 Molecular Docking

Docking experiments are a computational procedure that determines the position and binding mode of a protein-ligand complex minimum energy. It is commonly used in our group because of its usefulness for the design of drugs[11–14]. In this work, docking experiments were used to determine how our ligand binding mode is synthesized *in silico* in the Thermolysin pocket.
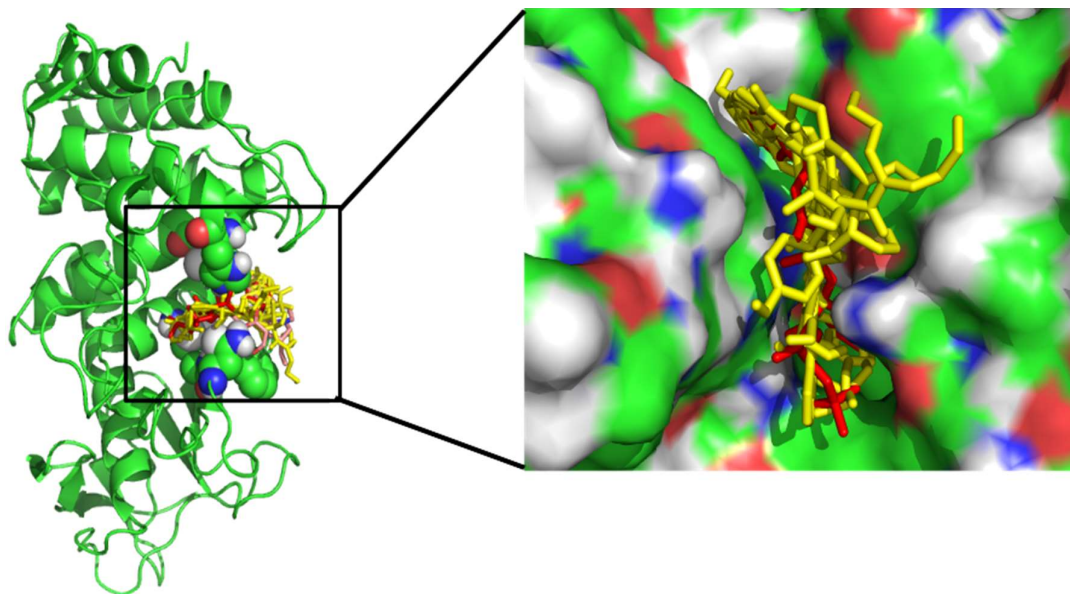


**Figure 1.** Best poses alignment of our ligands designed *in silico* (yellow) compared to 5H9 compound reference (red) into Thermolysin pocket.

As shown in Figure 1, the docking poses obtained were adjusted acceptably with available inhibitory X-ray crystal structures. All inhibitors were adequately targeted at the Thermolysin

pocket. In the docking experiments, the best poses were computed, and, as shown in Table 1, 86% of the poses obtained had a $\Delta G_{binding}$ greater than 7 kcal/mol, and 43% had an RMSD below 2 Å. The most stable complex of all was Lig5H9-5DPF, which presented the most negative free binding energy of all (-8.2 kcal/mol) and the second-lowest RMSD (Table 1) of all the complexes analyzed (0.90 Å). It is necessary to clarify that the RMSD values were obtained by comparing the complexes best poses with the crystallographic structure downloaded from the Protein Data Bank (PDB id:5DPF), so the reference ligand 5H9 was re-docked to have a validation of our docking experiments.

**Table 1.** Calculated docking $\Delta G_{binding}$ (kcal/mol) and RMSD (Å) of the firsts ranked Autodock Vina poses of Thermolysin-Ligand complexes.

| | Docking Pose-1 | | Docking Pose-2 | | Docking Pose-3 | |
|---|---|---|---|---|---|---|
| | $\Delta G_{binding}$ | RMSD | $\Delta G_{binding}$ | RMSD | $\Delta G_{binding}$ | RMSD |
| Lig5H9-5DPF [1] | -8.2 | 0.94 | -7.7 | 1.80 | -7.5 | 2.36 |
| Lig783-5DPF | -8.0 | 1.07 | -8.0 | 1.16 | -7.8 | 1.80 |
| Lig1022-5DPF | -7.9 | 0.90 | -7.8 | 1.88 | -7.7 | 1.46 |
| Lig1392-5DPF | -7.3 | 3.02 | -7.2 | 4.02 | -6.8 | 5.06 |
| Lig2177-5DPF | -8.0 | 2.45 | -7.9 | 3.01 | -7.8 | 3.76 |
| Lig3444-5DPF | -8.1 | 1.16 | -8.0 | 4.18 | -7.9 | 4.57 |
| Lig6199-5DPF | -7.0 | 6.76 | -6.9 | 6.81 | -6.6 | 6.85 |

[1]The 5H9 (N-[(S)-([(benzyloxy) carbonyl]amino methyl)(hydroxy)phosphoryl]-L-leucyl-4-methyl-L-leucine) is our reference molecule and was re-docked with the same docking procedure of the ligands studied.

A docking experiment detailed analysis reveals that the Lig5H9 presents a *POOH* group in its structure, which interacts by h-bond with the His231. This result reproduces what was found in the crystallographic structure obtained from the PDB and is further evidence of our result's validation (Figure 2A). Besides, the *C-OH* group interacts by h-bond with Arg203, and the *COOH* group also exhibits hydrogen bond interaction with Asn112, hence the excellent stability that this ligand presents in the active center of Thermolysin (Figure 2A).
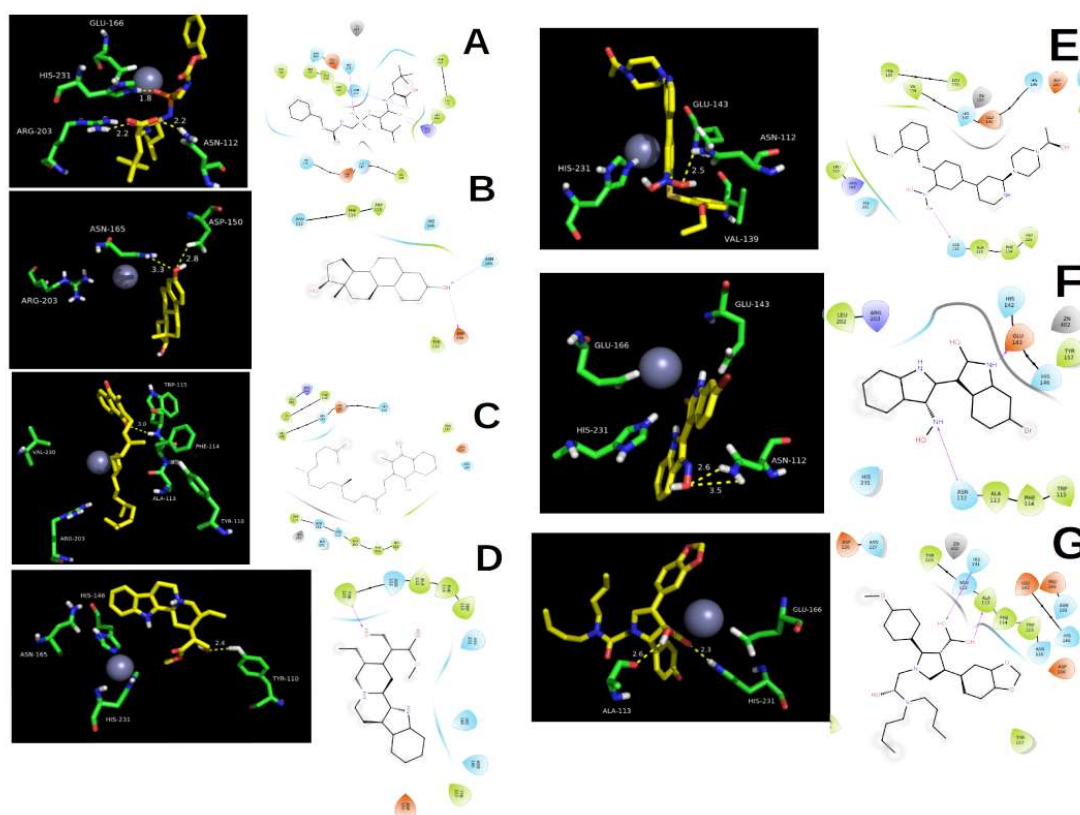
**Figure 2.** Binding modes structural details of the ligands designed *in silico* into the Thermolysin pocket: (A) 5H9 reference ligand, (B) Lig783, (C) Lig1022, (D) Lig1392, (E) Lig2177, (F) Lig3444 and (G) Lig-6199.

Of all the molecules designed *in silico*, the one that was best oriented in the Thermolysin pocket was Lig3444. The Lig3444-5DPF complex had the second most negative binding energy (counting the reference ligand 5H9) with a value of -8.1 kcal/mol, followed by Lig783 and Lig2177 with binding energies of -8.0 kcal/mol.

Another stable complex that was obtained in the docking experiments was Lig3444-5DPF. This ligand has a terminal *N-OH* group, which presents interactions by hydrogen bonding with Asn112. In addition to the fact that the pyrrolidine ring also presented h-bond interactions with Glu143, which gives it high stability to this complex (Figure 2 F).

The third and fourth place in the most negative binding free energy corresponded to ligands Lig783 and Lig2177, both with $\Delta G_{binding}$ of -8.0 kcal/mol. The Lig783-5DPF complex stability is due to this ligand present a terminal *C-OH* group in its structure, interacting by a hydrogen bond with Asp150 and Asn165. The molecule hydrocarbon skeleton was oriented into a hydrophobic pocket formed by Phe114, Trp115, and Trp157 (Figure 2 B). Lig2177 has a hydroxyl-amino group in its structure, which had a hydrogen bond interaction with Asn112. The terminal phenyl ring was oriented in a hydrophobic pocket formed by the Phe130. Leu133, and Val139, which gives it high stability to this complex (Figure 2 E).

These are the most stable ligands in docking experiments. To analyze if the interactions last over time, we will look at the molecular dynamics simulation results that will help us delve into this system's behavior at the molecular level over time.

*2.2 Molecular Dynamics Simulation.*

Molecular dynamics simulations give trajectories that contain structural information of thermolysin-ligand complexes at the molecular level[15–17]. Principally, our principal goal was focused on analyzing if the interactions found in the docking experiments are maintained over time. To obtain these results, we have performed an integral analysis of the data obtained from molecular dynamics simulations, which we show below.

*2.2.1 Root Means Squared Deviation (RMSD).*

As a stability criterion of the studied complexes, we will begin by analyzing the RMSD (Root Means Squared Deviation) parameter[18–20]. This variable will give us an idea of how the systems evolve during the 50 ns of simulation time. As shown in Figure 3, starting from the first 3 ns, all the complexes studied remained stable over time with a minimal appreciable variation. All the systems had RMSD values lower than 1.4 Å, even below the Lig5H9-5DPF complex (our reference system), indicating that the compounds designed *in silico* as possible antibacterials behaved stably over time into thermolysin pocket.

We can observe the RMSD parameter as the stability criterion of the studied systems in Table 2. There were no significant differences in the average value of the RMSD over time. The most stable complex was Lig2177-5DPF (0.90±0.07 Å). This system had the lowest RMSD value of all the complexes studied, even lower than our reference system (Lig5H9-5DPF), which had an average RMSD value of 1.11±0.13 Å.

**Table 2.** Average values and standard deviation of some parameters taken from 50 ns of trajectories.

| Complexes | RMSD (Å) | Number of H-bond | Rg (Å) |
|---|---|---|---|
| Lig5H9-5DPF [1] | 1,11 ± 0,13 | 1,48 ± 1,68 | 5,36 ± 0,52 |
| Lig783-5DPF | 0,93 ± 0,08 | 0,17 ± 0,54 | 3,56 ± 0,02 |
| Lig1022-5DPF | 1,02 ± 0,11 | 0,09 ± 0,32 | 5,88 ± 0,86 |
| Lig1392-5DPF | 1,10 ± 0,15 | 0,35 ± 0,82 | 4,25 ± 0,04 |
| Lig2177-5DPF | 0,90 ± 0,07 | 0,46 ± 0,73 | 5,78 ± 0,29 |
| Lig3444-5DPF | 0,98 ± 0,08 | 0,74 ± 1,26 | 3,87 ± 0,03 |
| Lig6199-5DPF | 0,97 ± 0,08 | 0,05 ± 0,26 | 4,99 ± 0,14 |

[1]The 5H9 (N-[(S)-([(benzyloxy) carbonyl]amino methyl)(hydroxy)phosphoryl]-L-leucyl-4-methyl-L-leucine) is our reference molecule and was re-docked with the same docking procedure of the ligands

It is important to note that the Lig2177-5DPF complex presented one of the most negative binding energies in the docking experiments (Table 1). The Lig783-5DPF, Lig6199-5DPF and Lig3444-5DPF complexes had RMSD values very close to the Lig2177-5DPF complex (0.93±0.08 Å, 0.97±0.05 Å and 0.98±0,07 Å respectively). Except for Lig6199-5DPF, the Lig783-5DPF and Lig3444-5DPF systems had very similar binding energies between each other and concerning the Lig2177-5DPF complex docking experiments.
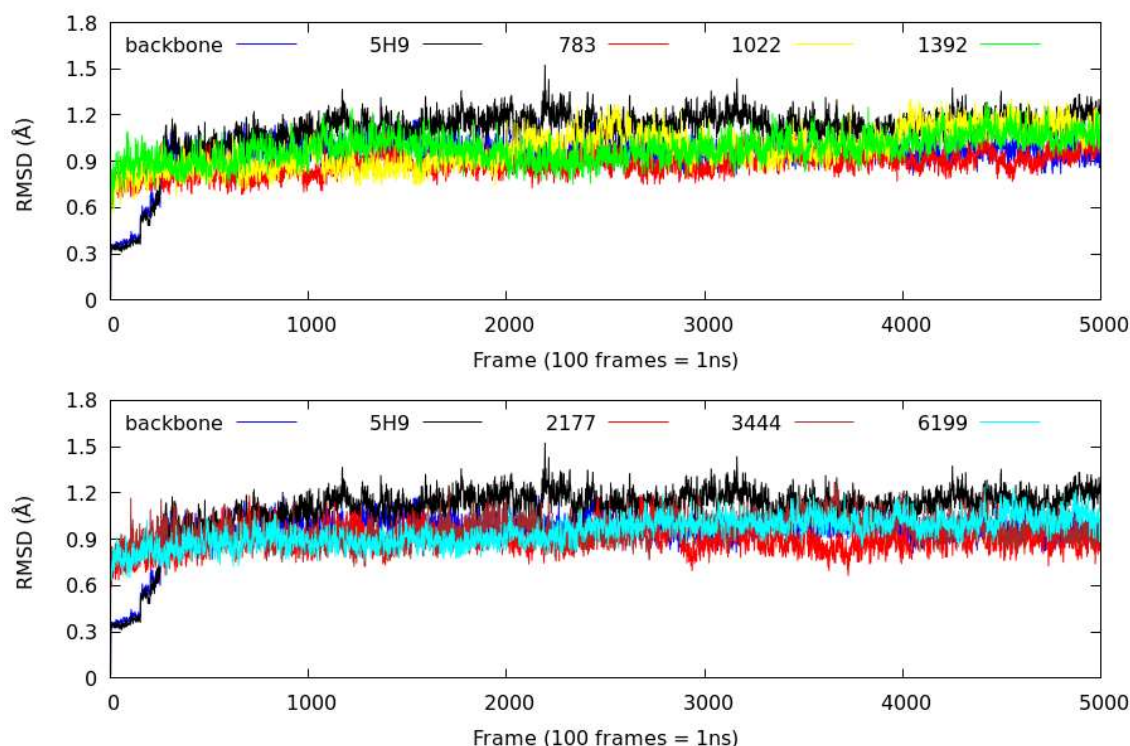
**Figure 3.** Comparative plots of RMSD values against simulation time corresponding to molecular dynamics of the backbone, 5H9 ligand reference, and molecules designed *in silico*-Thermolysin complexes.

The least stable complexes (which does not mean that they are unstable) were Lig1022-5DPF, Lig1392-5DPF, and our reference system Lig5H9-5DPF with RMSD values of 1,01±0,11 Å, 1,10±0,15 Å, and 1,11±0,13 Å, respectively. The standard deviation of this parameter for the mean value is very low.  This analysis indicates that the RMSD values were maintained with little fluctuation over time and is essential since the simulation time of these systems (50 ns) is sufficient to determine the binding mode of the *in silico* designed ligands in the active center of thermolysin. From the data obtained, we can conclude that the RMSD parameter did not detect significant differences in the dynamic behavior of the complexes studied. It is necessary to analyze details at the molecular level of the paths through the hydrogen bond's number and stability (h-bond). Analysis that we will carry out below.

### 2.2.2 Hydrogen bond interactions (H-bond).

We quantified the amount and occupancies of h-bond interactions during the 50 ns of simulation time to analyze the studied complex's stability. As shown in Figure 4, the number of h-bond interactions was low in all the complexes studied. None of the systems had an h-bond average higher than 1.5 (Table 2), indicating that these interactions do not significantly influence the complexes stability studied.

In addition to the low amount of h-bond, the stability of these interactions was also low. As shown in Table 2, the standard deviation of h-bond interactions for all the systems was higher than the population means, indicating the significant instability of these interactions. Another interesting fact that must be emphasized is the h-bond interaction occupancies over time. The occupancy term (%) refers to when the h-bond interaction is maintained less than 3 Å of distance during the 50 ns of simulation. Occupancy of more than 50% was taken as a stability criterion[21,22].
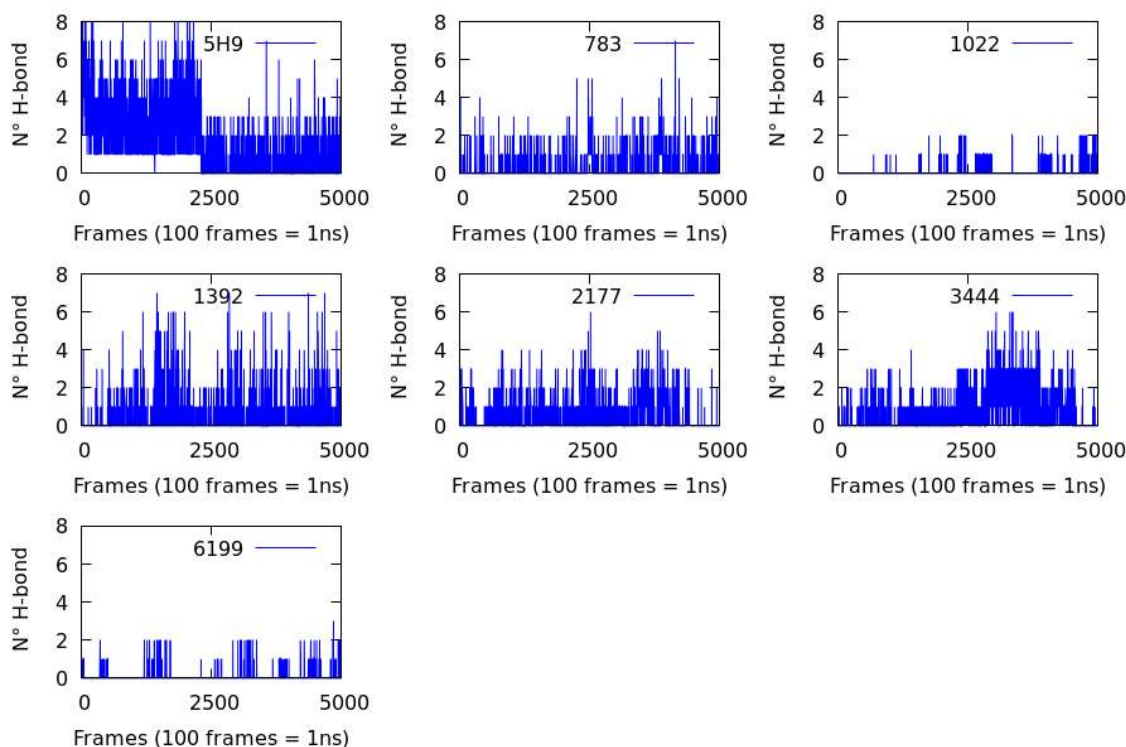
**Figure 4.** The number of hydrogen bonds between the Thermolysin and our ligands designed *in silico* during 50 ns of molecular dynamics simulation.

The highest occupancy was obtained from the hydrogen bond interaction formed by *Lig5H9-OH--O-Glu166*, maintained at an average distance of 1.75±2.38 Å the 24.63% during 50 ns of molecular dynamics simulation. The second-highest occupancy was found in the h-bond interaction formed by *Lig783-OH--O-Asp150*, which had 20.36% of occupancy 2.83±1.60 Å during the trajectory.

From this analysis, we can conclude that given the low amount of hydrogens and the instability of these interactions, we can not explain the complex stability shown in the molecular dynamics simulations using this parameter. For that reason, it is necessary to analyze other parameters such as radius of gyration, whose results we will present below.

### 2.2.3 Radius of Gyration (Rg).

The stability of the complexes analyzed using the RMSD parameter and h-bond interaction could not be explained. We will now analyze the compaction degree of 5DPF-ligand complexes during 50 ns of molecular dynamics trajectories. The compaction degree of the complexes studied will be addressed using the Radius of gyration (Rg) parameter[23–25]. This variable is defined as the root mean square distance of the mass of a collection of atoms from a common center of mass. The Rg graph leads to two analysis levels: the parameter's value over time and its fluctuation[23–25].
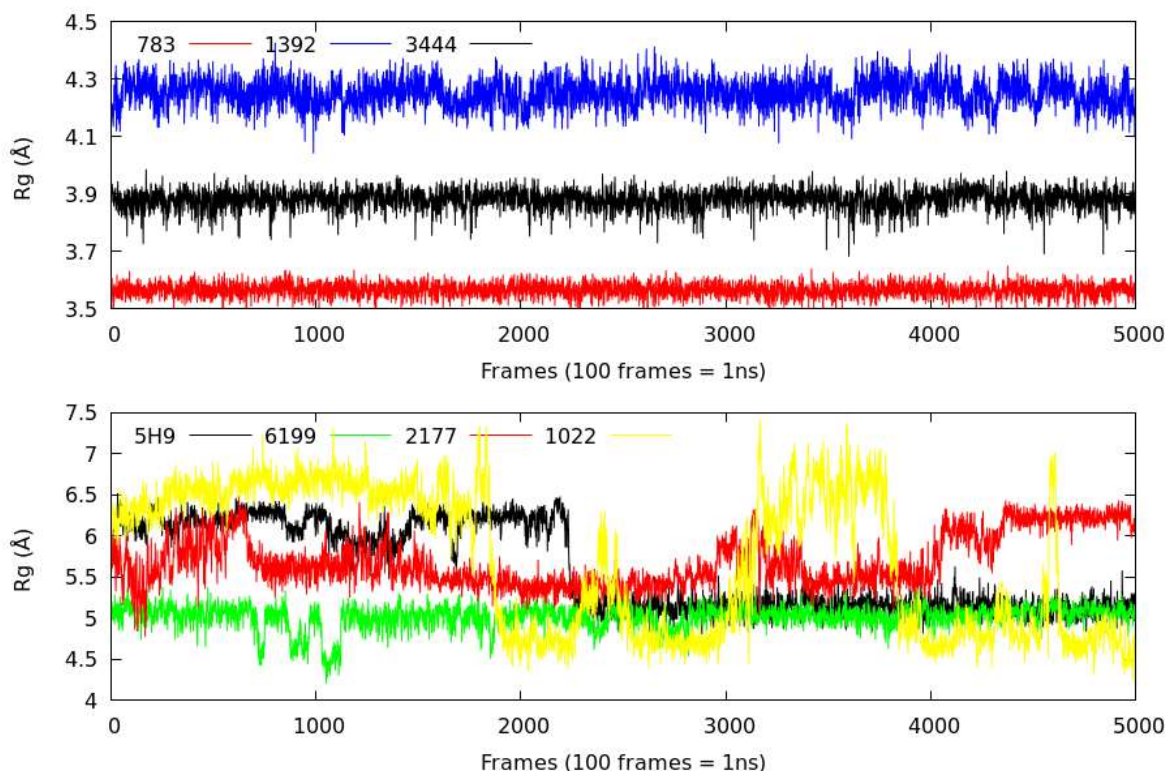
**Figure 5.** The gyration radius of C$\alpha$ atoms of the ligands-Thermolysin complexes during 50 ns of molecular dynamics simulation.

As shown in Figure 5, the complexes that remained more compact over time were Lig783-5DPF, Lig3444-5DPF, and Lig1392-5DPF. These systems had the lowest values and standard deviation of all the analyzed complexes (Table 2). These complexes remained stable over time without appreciable conformational changes during the 50 ns of simulation time. Another complex that remained compact overtime was the Lig6199-5DPF, although the Rg value was slightly higher than Lig783-5DPF, Lig3444-5DPF, and Lig1392-5DPF.

A very different behavior was obtained from the trajectory of the Lig5H9-5DPF, Lig1022-5DPF, and Lig2177-5DPF complexes. As shown in Figure 5, the complex formed by Lig5H9-5DPF had small conformational fluctuations during the first 22 ns of trajectory. From this simulation time, the system stabilizes until the end of the trajectory.

The Lig1022-5DPF complex behavior was different, which was the least compact of all systems studied with many fluctuations during 50 ns of simulation. As shown in Figure 5, this system had few fluctuations in the first 18 ns of simulation time. However, there was a conformational change (Figure 6) in which the radius value decreases abruptly. Then its value increases again from the nanosecond 33, demonstrating the low stability of this complex.
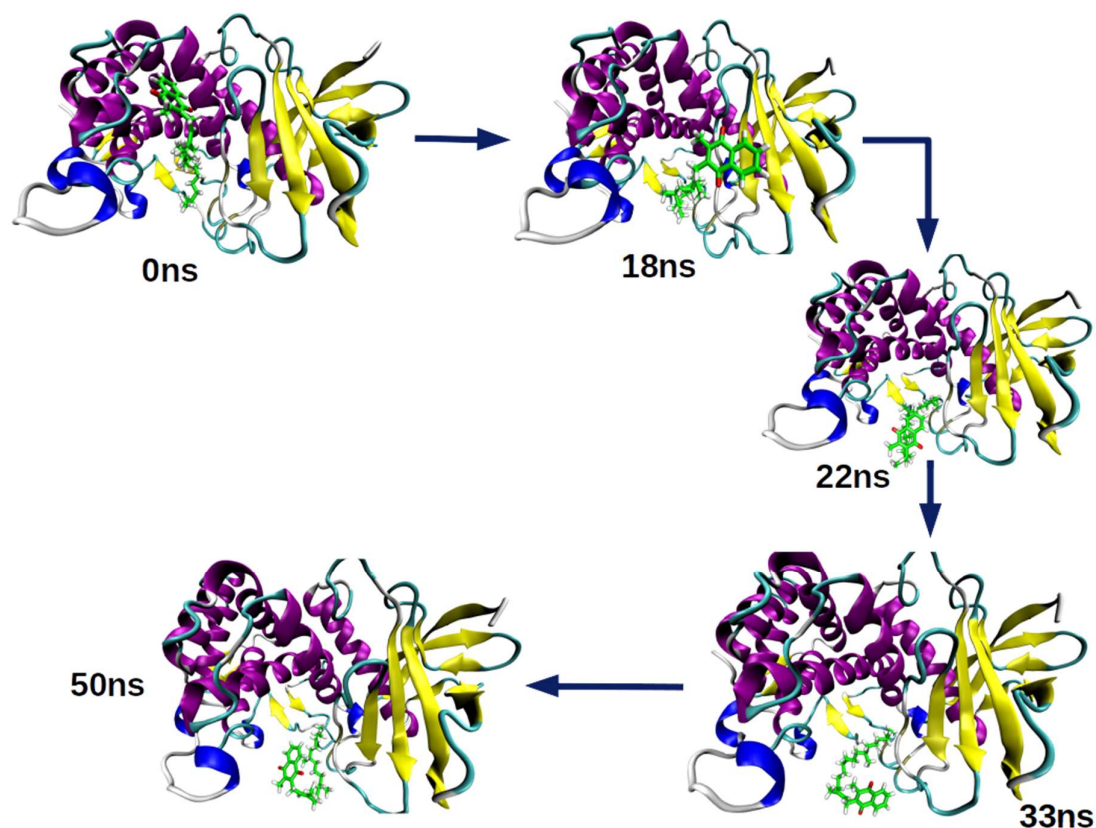
**Figure 6.** Conformational changes of Lig1022 during the 50 ns of molecular dynamics simulation.

*2.2.4 Root Mean Squared Fluctuation (RMSF).*

The root mean squared fluctuation (RMSF) parameter gives us a measure of the flexibility of the different residues composed of the Thermolysin structure during the trajectory[26]. At high RMSF values, there is greater flexibility of movement, and at low RMSF values indicates that there are movement restrictions during the simulation.

As shown in Figure 7, for all the complexes studied, the lowest RMSF values were found between amino acids 129-155 and 161-165, indicating that this area in contact with the designed ligands *in silico* remained more rigid than the reference. It is necessary to emphasize that this zone is the Thermolysin active center and the conserved sequence (HExxH) in the M4 family proteins[9,27], which in the case of this protein, the sequence is His142-Glu166-Tyr157-His146-His231. The most flexible amino acid residues were Asn183 and Glu199, which have a structural rather than a catalytic role.
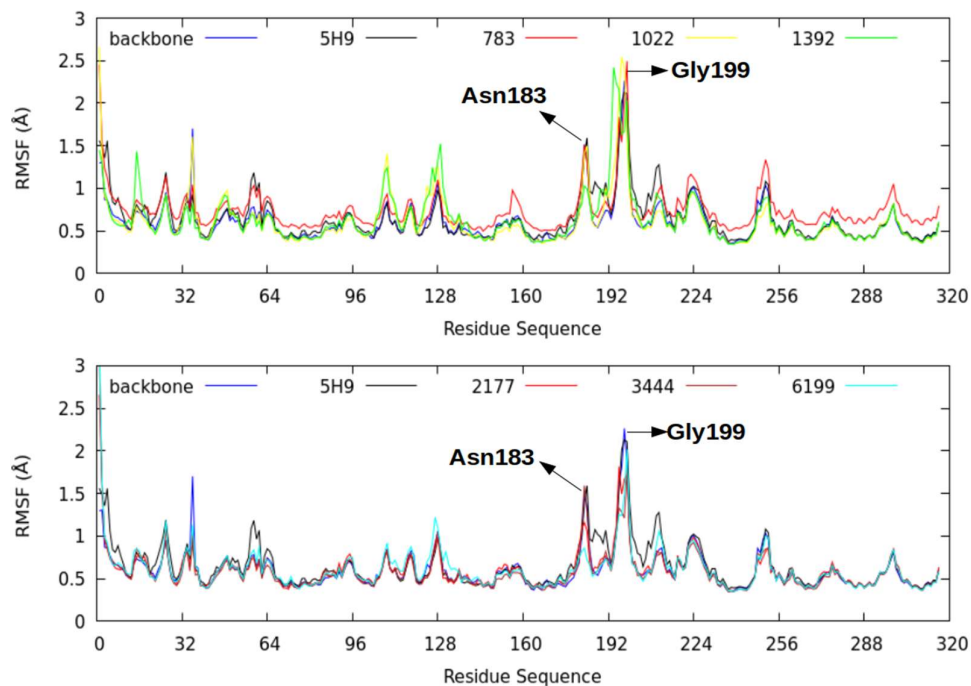
**Figure 7.** Root mean square fluctuation of the backbone atoms of the ligand-thermolysin complexes during 50 ns of molecular dynamics simulations at 298.15 K.

*2.3 MM-PBSA.*

The Molecular Mechanic Poisson-Boltzmann Surface Area (MM-PBSA) method will help us explore the molecular level at which energy components contribute favorably or unfavorably to the studied complexe's stability a free energy decomposition analysis[28].

**Table 3.** Predicted relative MM-PBSA free energies (kcal/mol) and individual energy contributions of the complexes taken from 50 ns of trajectories.

| Complexes | $\Delta G_{binding}$ | $\Delta E_{elect}$ | $\Delta E_{vdw}$ | $\Delta G_{polar}$ | $\Delta G_{Apolar}$ |
|---|---|---|---|---|---|
| Lig5H9-5DPF [1] | -146.79±8.30 | -150.45±13.06 | -227.00±7.61 | 254.72±9.29 | -24.05±0.74 |
| Lig783-5DPF | -60.84±11.32 | -24.72±14.56 | -81.13±0.29 | 55,27±17.78 | -10.26±0,84 |
| Lig1022-5DPF | -114.11±25.88 | -1.84±5.19 | -120.97±20.03 | 25.89±25.87 | -17.12±2.35 |
| Lig1392-5DPF | -75.79±11.25 | -23.69±6.66 | -87.35±8.27 | 46.35±12.71 | -11.09±1.40 |
| Lig2177-5DPF | -37.06±10.44 | -42.08±10.52 | -63.36±15.97 | 78.06±17.56 | -9.07±2.28 |
| Lig3444-5DPF | -27.31±11.72 | -7.94±6.26 | -49.88±20.82 | 36.92±21.27 | -6.41±2.67 |
| Lig6199-5DPF | -88.56±19.45 | -74,95±15.19 | -159.04±16.52 | 165.67±33.93 | -20.23±1.22 |

[1]The 5H9 (N-[(S)-([(benzyloxy) carbonyl]amino methyl)(hydroxy)phosphoryl]-L-leucyl-4-methyl-L-leucine) is our reference molecule and was re-docked with the same docking procedure of the ligands

As shown in Table 3, in general, the Van der Waals electrostatic and the nonpolar solvation terms contributed to the studied complex's stability. However, the $\Delta G_{polar}$ term behaved destabilizing in these systems (Table 3).

Of all the complexes studied the Lig5H9-5DPF had the most negative $\Delta G_{binding}$ value, indicating that it was the most stable complex of all, which agrees with that obtained in the docking experiments. This ligand in our reference was obtained from the Protein Data Bank.

The complex formed by Lig1022 with Thermolysin (Lig1022-5DPF) had the most negative binding energy of all the ligands designed *in silico*. This complex had the third most negative binding energy in docking experiments. According to the MMPBSA calculations results, Lig1022-5DPF is stabilized by Van der Waals interactions, which is the third most negative of all the complexes studied.

Lig6199 and Lig1392 were the complexes that had the second and third most negative $\Delta G_{binding}$, in MM-PBSA calculations. These systems had fewer negative energies in the docking experiments, which shows that they had losses of interactions during the molecular dynamics simulations. Like the Lig1022-5DPF complex, these two systems are mainly stabilized by Van der Waals interactions.
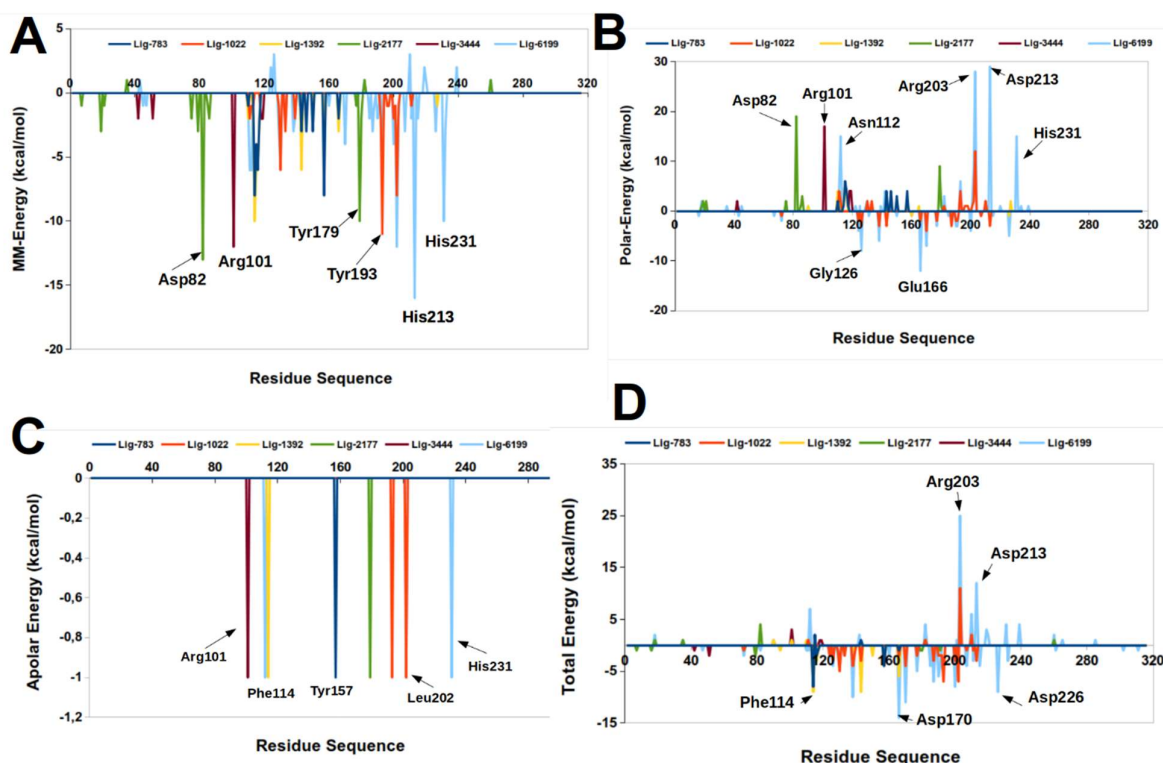


**Figure 8.** Decomposition of the binding free energy per residue basis on the Thermolysin pocket.

From the detailed analysis by residue (Figure 8), we can observe that the Phe126, Asp138, Glu166, Glu187, and Asp170 residues contributed favorably to $\Delta G_{binding}$. Note that Glu166 residue was found in the conserved sequence of the M4 family proteins active center[9,27] and has an essential catalytic role[9,27]. Molecular dynamics simulations, together with free energy calculations, corroborate this result.

The amino acids Asp82, Arg101, Asn112, Phe114, and His231 contributed favorably to the electrostatic origin and Van der Waals interactions. His231 is another essential amino acid present in the thermolysin active center and is within the consensus sequence of the M4 family proteins active center[9,27].

*2.4 Ligand Efficiency Calculation and ADME-Tox Properties.*

Until now, we have analyzed the molecular stability bases of the Thermolysin-ligand complexes. In the next section, we will analyze the affinity of the compounds designed *in silico* and Thermolysin and the ADME-Tox properties. These results will help us to discriminate which of the designed

compounds could be the best candidates for antibacterial agents, minimizing the risk as much as possible.

We have used in this analysis four parameters, the dissociation constant ($K_d$), ligand efficiency index (LE), binding efficiency index (BEI), and lipophilic ligand efficiency (LLE), which will help us compare and select the best candidates for antibacterial agents. The dissociation constant ($K_d$) parameter gives us a measure of how strong or weak is the ligand-Protein interaction. Low values indicate a strong interaction between the ligand and the protein. The dissociation constant was calculated using Equation 4. As shown in Table 4, the most robust interaction was obtained with Lig5H9, which presented significant differences with the rest of the ligands studied. Of the compounds designed *in silico*, Lig3444, Lig783, and Lig2177 had the lowest $K_d$ values, indicating that they could be good candidates for antibacterial agents.

**Table 4.** Ligand efficiency parameters calculated and ADME-Tox properties prediction for all molecules studied.

| Ligands | MW (kDa) | $K_d$ | clogP | LE | BEI | LLE | HBA | HBD | TPSA ($\mathring{A}^2$) | RB |
|---------|----------|-------|-------|-----|------|------|-----|-----|------|-----|
| Lig5H9 [1] | 0.4855 | $9.78 \times 10^{-7}$ | 2.71 | 0.248 | 12.37 | 3.29 | 8 | 5 | 163.87 | 16 |
| Lig783 | 0.2723 | $1.37 \times 10^{-6}$ | 2.60 | 0.400 | 21.52 | 3.26 | 2 | 2 | 40.46 | 0 |
| Lig1022 | 0.4507 | $1.62 \times 10^{-6}$ | 5.86 | 0.239 | 12.84 | -0.07 | 2 | 0 | 34.14 | 14 |
| Lig1392 | 0.3574 | $4.46 \times 10^{-6}$ | 2.81 | 0.280 | 14.96 | 2.54 | 3 | 3 | 74.35 | 5 |
| Lig2177 | 0.4805 | $1.37 \times 10^{-6}$ | 3.45 | 0.235 | 12.19 | 2.41 | 5 | 2 | 114.67 | 0 |
| Lig3444 | 0.3561 | $1.15 \times 10^{-6}$ | 2.31 | 0.368 | 16.66 | 3.62 | 3 | 3 | 74.72 | 0 |
| Lig6199 | 0.5106 | $7.64 \times 10^{-6}$ | 4.06 | 0.189 | 10.04 | 1.07 | 7 | 1 | 88.56 | 13 |

[1]The 5H9 (N-[(S)-([(benzyloxy) carbonyl]amino methyl)(hydroxy)phosphoryl]-L-leucyl-4-methyl-L-leucine) is our reference molecule and was re-docked with the same docking procedure of the ligands.

The ligand efficiency index (LE) is a parameter that correlates the ligand-Protein binding energy and the number of atoms in the compound without taking into account the hydrogens in its structure[29]. In our work, we take LE>0,3 kcal/mol HAC as a reference for an adequate drug candidate[29–31]. Consistent with the reference value, compounds Lig783 and Lig3444 are good candidates as thermolysin inhibitors since they had LE values of 0,40 and 0,36, respectively (Table 4). Studies carried out on common drugs have given LE values between 0.5 and 0.52 for drugs for oral administration[29], so we can suggest that the compounds Lig783 and Lig3444 could be good candidates for orally administered drugs.

The binding efficiency index (BEI) is a parameter that relates the dissociation constant ($K_d$) of the ligand and its molecular weight[32]. As reference values for this parameter, we have taken 20<BEI<27. These values were obtained from drugs known as Bortezomid (BEI=21)[33]. Our ligand's BEI values were low compared to the reference values; only Lig783 had a BEI value similar to Bortezomib, a commercially available proteasome inhibitor[33]. Our ligand's low BEI values designed *in silico* are because of the compound high molecular weight.

Another essential variable to analyze is lipophilic ligand efficiency (LLE). This parameter measures the ligand-binding capacity with the protein and its lipophilic power[29]. In our case, LLE's reference values are taken between 5-7 units, values calculated in known drugs for oral administration[34]. As shown in Table 4, the ligands designed *in silico* obtained LLE values lower than the reference values, mainly due to the relatively high values of the cLogP variable, which means that these compounds have high lipophilic power (Table 4). Suppose we stop to analyze the

chemical structure of our molecules (Figure 10). In that case, we can observe that they have apolar hydrocarbon skeletons, which could influence our lipophilic ligand capacity.

For a promising drug candidate molecule, the pharmacokinetics prediction (absorption, distribution, metabolism, and elimination (ADME)) is necessary. Also, some toxicological parameters (Tox)[35–38] will be critical to known. In this work, we calculated the molecular weight (MW), the octanol/water partition coefficient (cLogP), hydrogen bond acceptor count (HBA), hydrogen bond donor count (HDA), and rotatable bond count (RB) for each one of the molecules studied using SwissADME web server[39]. As a toxicological criterion, these results were compared with the Lipinski[40], Veber[41], and Pfizer[42] rules. Thus, if any compounds designed *in silico* comply with only one Lipinski rule, this compound would not be the right candidate. On the contrary, according to the Veber and Pfizer rules, a right ligand candidate must comply with both rules in both cases.

As shown in Table 4, our reference ligand 5H9 meets all the parameters of the Lipinski Rule. However, it does not meet any of the parameters of the Veber rule. It only meets one of the parameters of the Pfizer Rule, indicating that this compound could have high oral availability. However, its high lipophilic power could have some toxicological potential. The compounds Lig783, Lig1392, and Lig3444 comply with all the Lipinski, Veber, and Pfizer rulers, so we consider these ligands the best antibacterial candidate agents. The Lig1022, Lig2177, and Lig6199 molecules result in not good candidates because of the high lipophilic power. This parameter provokes some toxicological consequences.

## 3. Computational Protocol.

In this work, we planned a computational biochemistry protocol to evaluate Thermolysin inhibitors as possible antibacterial agents, as shown in Figure 9.
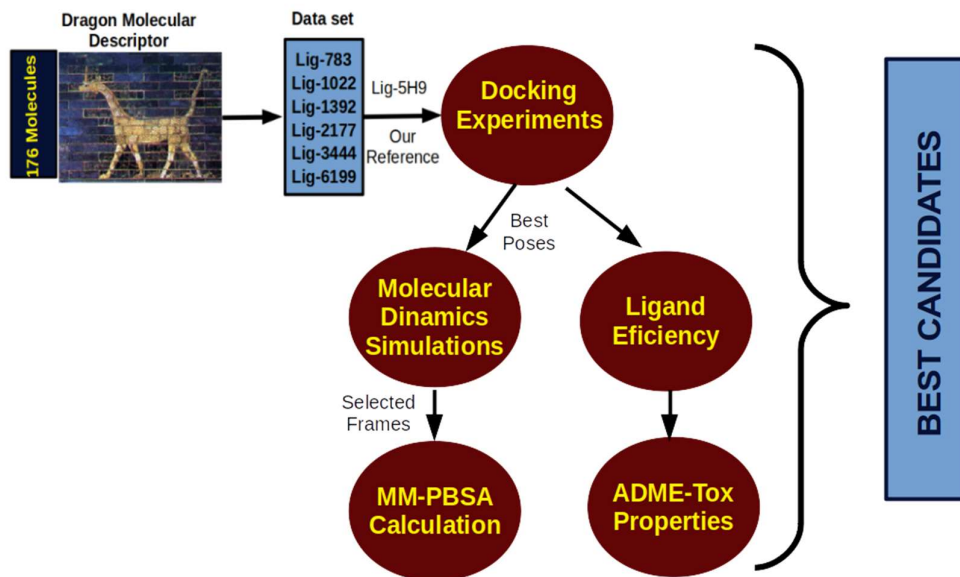


**Figure 9.** Computational protocol for evaluation of possible antibacterial agents.

The molecules that we will study in this work were designed by our group using the QSARIN method reported in previous works[11]. The molecular structures of these possible Thermolysin inhibitors were sketched using Avogadro software version 1.2.0[43]. The optimized geometry was obtained using DFT calculation at the b3lyp/ma-def2-SVP basis set implemented in Orca 4.2.1 software package[44,45]. The full optimized geometry was checked by counting their imaginary frequencies. The molecular structure of the Thermolysin inhibitors studied is represented in Figure

10. The optimized geometries of these molecules were obtained for docking experiments to examine the interactions of these compounds in the Thermolysin pocket.
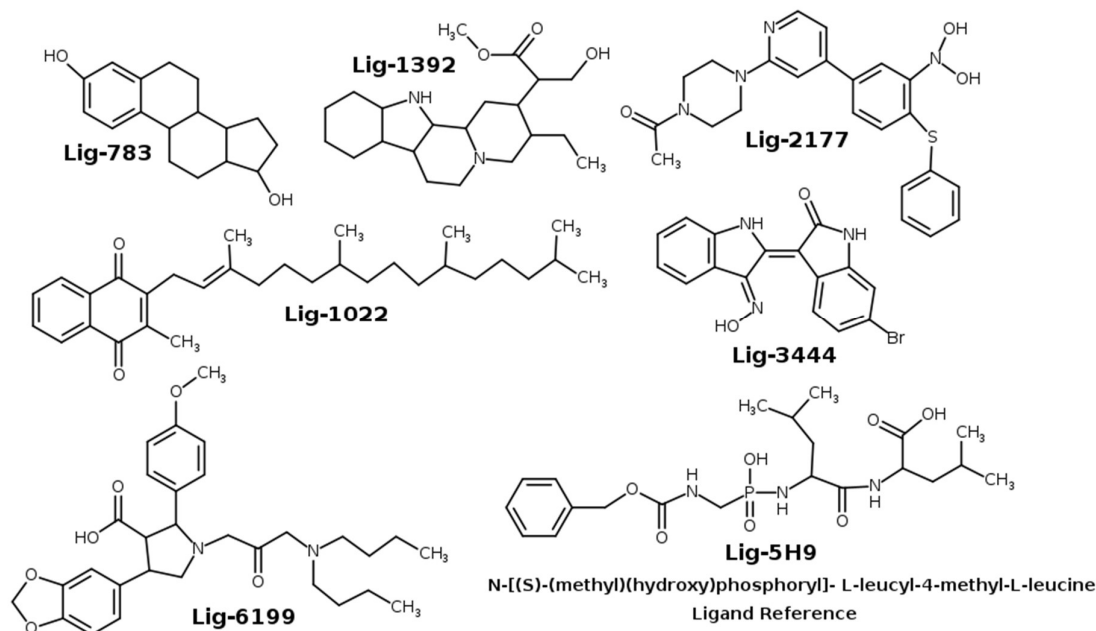


**Figure 10.** Molecular structure of Thermolysin inhibitors as possible antibacterial agents.

### 3.1 Docking Procedure.

The full optimized geometry obtained from the quantum calculation of the ligands were used for docking experiments. The molecules were prepared at pH=7.4 using Autodock Tools[46]. The X-ray crystallography structure of Thermolysin was obtained from Protein Data Bank (PDB)[47] from *Bacillus thermoproteolyticus*, whose PDBid is 5DPF, resolved at 1.47 Å[48]. This protein was prepared by the addition of all hydrogen atoms at pH=7.4. The water molecules around the protein were eliminated. The size of the grid box was 16.875×14.14×16.875 Å around the mass centers of the 5H9 our reference ligands discharged from x-ray crystallography structure from PDB whose coordinates were x = 11,844 y=-40,829 and z = 6,420. The Thermolysin is an M4 family of proteinases with $Zn^{2+}$ into the pocket, that´s why we kept this element in all docking experiments.

In all docking procedures, we used a grid spacing of 0.375 Å, the number of modes was 10, and the energy rank was set up to 1 kcal/mol. To analyze if our docking results were correct, the 5H9 reference ligand was re-docked using the same docking protocol of the other compounds. All docking experiments were realized with Autodock Vina software version 1.1.2[49,50]. The best docking poses were selected using binding energy (kcal/mol) and the positional root-mean-square deviation (RMSD)[51].

The best energetically good poses and lowest root-mean-square deviation of each complex were selected for molecular dynamics simulations and ligand efficiency calculations. To verify the docking results reproducibility, we calculate the root-mean-square deviation (RMSD), between the possible antibacterial compounds, taking 5H9 as ligand reference from the crystallographic structure of Protein Data Bank. These calculations were realized using the LigRMSD server 1.0 program[52]. All docking figures were made using Pymol software version 1.8[53].

### 3.2 Molecular Dynamics Simulation.

We obtained the best conformational poses for each ligand-Thermolysin complex from docking experiments as input for molecular dynamics simulations. Each complex was placed into a water box of 15×15×15 Å, using the TIP3P water model[54,55]. Topologies and parameters of the ligands were obtained by the SwissParam web Server[56]. All molecular dynamics simulations were described using CHARMM36 and CGenFF force field for the Thermolysin and the possible antibacterial compounds[57–61].

The ligand-Thermolysin complexes were submitted to 50000 steps for the energy minimization using the conjugated gradient methodology for reducing any close contact. The working temperature was 298.15 K employing the weak coupling algorithm[62]. The Van der Waals cutoff was fixed to 12 Å, and we applied a backbone constraint to all complexes using the NPT ensemble. The Particle Mesh Ewald (PME) approach[63] was used for considering the long ranges of electrostatic forces. We employed the velocity Verlet algorithm with a time step of 1.0 fs to solve the motion equations. All the complexes were submitted to 2.0 ns of equilibration and 50 ns of molecular dynamics simulation using the NAMD 2.13 software package[64]. The trajectories analysis and scripts were realized using the VMD software version 1.9.3[65].

### 3.3 Free energy Calculation.

This work's computational protocol combines molecular dynamics simulation and MM-PBSA to study the ligands and Thermolysin interactions. The binding free energy was calculated using *g_mmpbsa* package version 5.1.2[66], a Gromacs tool to compute the ligand-free binding energy[66]. This is an implicit solvent method that computes the different energy between the ligands-Thermolysin complexes.

From 50 ns of molecular dynamics simulation, we extract the last 300 frames to compute each binding free energy of complexes. So the MM-PBSA method calculates the free energy decomposition into contributions. The free energy for the Thermollysin–ligand complexes were calculated according to the following equation:

$$\Delta G_{binding} = G_{complex} - \left( G_{Thermolysin} + G_{ligand} \right) \tag{1}$$

In Equation 1 $G_{complex}$ corresponds to the Thermolysin-ligand complex energy, $G_{Thermolysin}$, and $G_{ligand}$ is the energy of protein and ligand respectively. The following equation was used to calculate the free energy of the protein, ligand, and complex separately.

$$G_x = E_{bond} + E_{vdw} + E_{elect} + G_{polar} + G_{Apolar} \tag{2}$$

In the Equation, 2 $G_x$ can be $G_{complex}$ or $G_{Thermolysin}$, or $G_{ligand}$. The $E_{bond}$ represents the interactions that include bond, angle, and dihedral angle, $E_{elect}$ is the electrostatic energy contribution, $E_{vdw}$ is a Van der Waals energy contribution. The $G_{polar}$ represents the polar free energy contribution, which was calculated using the continuum solvent Poisson-Boltzmann (PB) model included in the APBS (Adaptive Poisson-Boltzmann Solver) software version 1.4.1[67]. The non-polar free energy contribution was calculated according to the following equation:

$$G_{Apolar} = \gamma SASA + \beta \tag{3}$$

where $\gamma$ represent the coefficient related to the surface tension of the solvent, which in our case has a value of 0.0072 kcal/mol/Å², SASA is the solvent-accessible surface area, with an amount of 1.4 Å and $\beta$ is a fitting parameter.

We also decompose the overall binding energy per residue because we need to know every amino acid contribution. These contributions were calculated using pythons script *MmPbSaStat.py*, and the

individual contribution of various amino acids in binding is calculated by *MmPbSaDecomp.py* scripts[66].

### 3.4 Ligand Efficiency Calculation.

Ligand efficiency metrics consist of a series of parameters that seek to measure the relationship between the binding energy and the molecule size[29]. These parameters have currently taken on important relevance in predicting how efficient a given compound will be as a possible drug[29,31,68,69]. In our case, the ligand efficiency calculations were performed through several parameters, such as the dissociation constant ($K_d$), the ligand efficiency index (LE), the binding efficiency index (BEI), and the lipophilic ligand efficiency (LLE).

The $K_d$ corresponds to the dissociation constant between a ligand and the protein. Its value indicates the bond strength between the ligand and the protein[31,68]. The following equations calculated this parameter:

$$K_d = 10^{\left[\frac{\Delta G_{docking}}{2,303RT}\right]} \tag{4}$$

According to Equation 4, $\Delta G_{docking}$ is the binding energy (kcal/mol) obtained from docking experiments, R is the gas constant whose value is 0,001987 kcal/molK, and T is the temperature in Kelvin, in our case, 298.15 K.

Ligand efficiency index (LE) is a measure of the binding energy and the compound's size [31,70]. This parameter allows us to compare molecules according to their average binding energy and can be calculated according to the following equation[31]:

$$LE = \frac{-2,303RT}{HAC} \log(K_d) \tag{5}$$

In Equation 5 $K_d$ is the dissociation constant calculated from Equation 4, and HAC corresponds to the number of non-hydrogen atoms (heavy atom counter) in a ligand.

Binding efficiency index BEI is a measure that involves a binding property of the ligand with the protein against molecular weight[71,72]. In this work, the binding efficiency index was calculated through the following equation[32]:

$$BEI = [pK_d MW] \tag{6}$$

where $pK_d$ is $-\log K_d$ and $K_d$ is the dissociation constant calculated from Equation 4. MW represents the molecular weight in kDa.

Lipophilic ligand efficiency (LLE) has been defined as the difference between the ligand activity and lipophilicity (clogP), as shown in Equation 7[73].

$$LLE = pK_d - clog(P) \tag{7}$$

In Equation 7 $pK_d$ is $-\log K_d$ and clogP is a ligand Lipophility measure, which was calculated employing SwissADME web server[39].

### 3.5 ADME-Tox Properties.

The absorption, distribution, metabolism, and excretion (ADME) properties of all ligands studied in this work were calculated from the molecules under study's optimized geometry, using the SwissADME web server[39]. We also calculated other physicochemical variables like molecular weight (MW), octanol/water partition coefficient (cLogP), hydrogen bond acceptor (HBA), hydrogen bond donor (HBD), topological polar surface area (TPSA), and rotatable bond count (RB) respectively. His fundamental goal is to obtain ties of a compound to become a drug. From these physicochemical parameters, we can predict the drug's toxicological properties (Tox) considering the Lipinski[40,74], Veber[41] , and Pfizer toxicity empirical rules[42] (Table 5).

**Table 5.** Empirical rules for predicting oral availability and toxicity properties of ligands studied.

| Properties | Oral Availability | | Toxicity |
| --- | --- | --- | --- |
| | **Lipinski Rules** | **Veber Rules** | **Pfizer 3/75 Rules** |
| **MW** | ≤500 | - | - |
| **cLogP** | ≤5 | - | ≤3 |
| **HBA** | ≤10 | - | - |
| **HBD** | ≤5 | - | - |
| **TPSA** | - | ≤140 | ≤75 |
| **RB** | - | ≤10 | - |

MW: Molecular weight; LogP: Octanol/water partition coefficient; HBA: Hydrogen bond acceptor; HBD: Hydrogen bond donor; TPSA: Topological polar surface area; RB: Rotatable bond count.

## 4. Conclusions

Bacterial diseases have increased around the world. This type of disease is caused by a large group of Gram-Positive, and Gram-Negative bacteria, which have M4 family metalloproteins containing $Zn^{2+}$ in their active center. This family of proteins is the cause of the bacteria's virulence. In previous works, we designed a series of Thermolysin inhibitor ligands (M4 family metalloproteinase). How can we determine if these designed compounds would be good antibacterial agents? In this work, we have successfully designed a computational protocol with a comprehensive analysis of the results obtained from docking experiments, molecular dynamics simulations, MM-PBSA, ligand efficiency calculation, and ADME-Tox prediction. From the results, we can conclude that the compounds Lig783, Lig2177, and Lig3444 were the ones that had the best behavior in the docking experiments. These same compounds had a very similar behavior during the 50 ns of molecular dynamics and MM-PBSA. These results coincided with the ligand efficiency analysis, demonstrating that these molecules can be good antibacterial agents. However, if we analyze the results extracted from the ADME-Tox properties, we can conclude that the best candidate is Lig783.

**Author Contributions:** K.M.U and EL. Conceived and designed the study. F.P.M conceived and realized the docking experiments and Molecular Dynamics Simulation, D.M.C realized the MM-PBSA calculation, E.L. performed the Ligand Efficiency Calculation, and drafted the first version of the paper, K.M.U., conceived and realized the ADME-Tox properties and contributed to the revision process of the manuscript and submit the paper. All authors reviewed the manuscript.

**Conflicts of Interest:** The authors declare no conflict of interest.

## References

1. 1.  Hoed, C.M. den; Kuipers, E.J. 45 - Helicobacter pylori Infection. In *Hunter's Tropical Medicine and Emerging Infectious Diseases (Tenth Edition)*; Ryan, E.T., Hill, D.R., Solomon, T., Aronson, N.E., Endy, T.P., Eds.; Content Repository Only! London, 2020; pp. 476–480 ISBN 978-0-323-55512-8.

2. 2.  WHO *2019 antibacterial agents in clinical development: an analysis of the antibacterial clinical development pipeline.*; 2019;

3. 3.  Huang, J.; Zeng, B.; Liu, D.; Wu, R.; Zhang, J.; Liao, B.; He, H.; Bian, F. Classification and structural insight into vibriolysin-like proteases of Vibrio pathogenicity. *Microb. Pathog.* **2018**, *117*, 335–340, doi:https://doi.org/10.1016/j.micpath.2018.03.002.

4. 4.  Howell, M.; Dumitrescu, D.G.; Blankenship, L.R.; Herkert, D.; Hatzios, S.K. Functional characterization of a subtilisin-like serine protease from Vibrio cholerae. *J. Biol. Chem.* **2019**, *294*, 9888–9900, doi:10.1074/jbc.RA119.007745.

5. 5.  Kavitt, R.T.; Lipowska, A.M.; Anyane-Yeboa, A.; Gralnek, I.M. Diagnosis and Treatment of Peptic Ulcer Disease. *Am. J. Med.* **2019**, *132*, 447–456, doi:https://doi.org/10.1016/j.amjmed.2018.12.009.

6. 6.  Vinasco, K.; Mitchell, H.M.; Kaakoush, N.O.; Castaño-Rodríguez, N. Microbial carcinogenesis: Lactic acid bacteria in gastric cancer. *Biochim. Biophys. Acta - Rev. Cancer* **2019**, *1872*, 188309, doi:https://doi.org/10.1016/j.bbcan.2019.07.004.

7. 7.  Khan, M.T.H.; Fuskevåg, O.-M.; Sylte, I. Discovery of Potent Thermolysin Inhibitors Using Structure Based Virtual Screening and Binding Assays. *J. Med. Chem.* **2009**, *52*, 48–61, doi:10.1021/jm8008019.

8. 8.  Goblirsch, B.R.; Wiener, M.C. Ste24: An Integral Membrane Protein Zinc Metalloprotease with Provocative Structure and Emergent Biology. *J. Mol. Biol.* **2020**, doi:https://doi.org/10.1016/j.jmb.2020.03.016.

9. 9.  Ezawa, T.; Saito, R.; Suzuki, S.; Sugiyama, S.; Sylte, I.; Kurita, N. Protonation states of central amino acids in a zinc metalloprotease complexed with inhibitor: Molecular mechanics optimizations and ab initio molecular orbital calculations. *Biophys. Chem.* **2020**, *261*, 106368, doi:https://doi.org/10.1016/j.bpc.2020.106368.

10. 10. Theuretzbacher, U.; Gottwalt, S.; Beyer, P.; Butler, M.; Czaplewski, L.; Lienhardt, C.; Moja, L.; Paul, M.; Paulin, S.; Rex, J.H.; et al. Analysis of the clinical antibacterial and antituberculosis pipeline. *Lancet Infect. Dis.* 2019, *19*, e40–e50.

11. 11. Cañizares-Carmenate, Y.; Mena-Ulecia, K.; Perera-Sardiña, Y.; Torrens, F.; Castillo-Garit, J.A. An approach to identify new antihypertensive agents using Thermolysin as model: In silico study based on QSARINS and docking. *Arab. J. Chem.* **2019**, *12*, 4861–4877, doi:10.1016/j.arabjc.2016.10.003.

32  12.  MacLeod-Carey, D.; Solis-Céspedes, E.; Lamazares, E.; Mena-Ulecia, K. Evaluation of new
33      antihypertensive drugs designed in silico using Thermolysin as a target. *Saudi Pharm. J.* **2020**, *28*, 582–
34      592, doi:10.1016/j.jsps.2020.03.010.

35  13.  Mena-Ulecia, K.; MacLeod-Carey, D. Interactions of 2-phenyl-benzotriazole xenobiotic compounds with
36      human Cytochrome P450-CYP1A1 by means of docking, molecular dynamics simulations and MM-
37      GBSA calculations. *Comput. Biol. Chem.* **2018**, *74*, 253–262, doi:10.1016/j.compbiolchem.2018.04.004.

38  14.  Quesada-Romero, L.; Mena-Ulecia, K.; Zuñiga, M. Pedro De-la-Torre, Daniela Rossi c, William Tiznado
39      b, Simona Collina c and Julio Caballero.

40  15.  Salsbury, F.R. Molecular dynamics simulations of protein dynamics and their relevance to drug
41      discovery. *Curr. Opin. Pharmacol.* **2010**, *10*, 738–44, doi:10.1016/j.coph.2010.09.016.

42  16.  Rivail, L.; Chipot, C.; Maigret, B.; Bestel, I.; Sicsic, S.; Tarek, M. Large-scale molecular dynamics of a G
43      protein-coupled receptor, the human 5-HT4 serotonin receptor, in a lipid bilayer. *J. Mol. Struct.*
44      *THEOCHEM* **2007**, *817*, 19–26, doi:10.1016/j.theochem.2007.04.012.

45  17.  Bocharov, D.; Krack, M.; Rafalskij, Y.; Kuzmin, A.; Purans, J. Ab initio molecular dynamics simulations
46      of negative thermal expansion in ScF3: The effect of the supercell size. *Comput. Mater. Sci.* **2020**, *171*,
47      109198, doi:10.1016/j.commatsci.2019.109198.

48  18.  Fegan, S.K.; Thachuk, M. A charge moving algorithm for molecular dynamics simulations of gas-phase
49      proteins. *J. Chem. Theory Comput.* **2013**, *9*, 2531–2539, doi:10.1021/ct300906a.

50  19.  Velázquez-Libera, J.L.; Durán-Verdugo, F.; Valdés-Jiménez, A.; Núñez-Vivanco, G.; Caballero, J.
51      LigRMSD: a web server for automatic structure matching and RMSD calculations among identical and
52      similar compounds in protein-ligand docking. *Bioinformatics* **2020**, doi:10.1093/bioinformatics/btaa018.

53  20.  Bell, E.W.; Zhang, Y. DockRMSD: An open-source tool for atom mapping and RMSD calculation of
54      symmetric molecules through graph isomorphism. *J. Cheminform.* **2019**, *11*, 40, doi:10.1186/s13321-019-
55      0362-7.

56  21.  Mena-ulecia, K.; Vergara-Jaque, A.; Poblete, H.; Tiznado, W.; Caballero, J. Study of the Affinity between
57      the Protein Kinase PKA and Peptide Substrates Derived from Kemptide Using Molecular Dynamics
58      Simulations and MM / GBSA. *PLoS One* **2014**, *9*, e109639, doi:10.1371/journal.pone.0109639.

59  22.  Mena-Ulecia, K.; Tiznado, W.; Caballero, J. Study of the Differential Activity of Thrombin Inhibitors
60      Using Docking, QSAR, Molecular Dynamics, and MM-GBSA. *PLoS One* **2015**, *10*, e0142774,
61      doi:10.1371/journal.pone.0142774.

62  23.  Kumar, K.M.; Anbarasu, A.; Ramaiah, S. Molecular docking and molecular dynamics studies on β-
63      lactamases and penicillin binding proteins. *Mol. Biosyst.* **2014**, *10*, 891–900, doi:10.1039/c3mb70537d.

64    24.    Kumar, A.; Purohit, R. Use of Long Term Molecular Dynamics Simulation in Predicting Cancer
65            Associated SNPs. *PLoS Comput. Biol.* **2014**, *10*, doi:10.1371/journal.pcbi.1003318.

66    25.    Lavanya, P.; Ramaiah, S.; Anbarasu, A. A Molecular Docking and Dynamics Study to Screen Potent Anti-
67            Staphylococcal Compounds Against Ceftaroline Resistant MRSA. *J. Cell. Biochem.* **2016**, *117*, 542–548,
68            doi:10.1002/jcb.25307.

69    26.    Mohammad, A.; Marafie, S.K.; Alshawaf, E.; Abu-Farha, M.; Abubaker, J.; Al-Mulla, F. Structural
70            analysis of ACE2 variant N720D demonstrates a higher binding affinity to TMPRSS2. *Life Sci.* **2020**, *259*,
71            118219, doi:10.1016/j.lfs.2020.118219.

72    27.    Eisenhardt, M.; Schlupp, P.; Höfer, F.; Schmidts, T.; Hoffmann, D.; Czermak, P.; Pöppel, A.-K.;
73            Vilcinskas, A.; Runkel, F. The therapeutic potential of the insect metalloproteinase inhibitor against
74            infections caused by Pseudomonas aeruginosa. *J. Pharm. Pharmacol.* **2019**, *71*, 316–328,
75            doi:10.1111/jphp.13034.

76    28.    Wang, E.; Sun, H.; Wang, J.; Wang, Z.; Liu, H.; Zhang, J.Z.H.; Hou, T. End-Point Binding Free Energy
77            Calculation with MM/PBSA and MM/GBSA: Strategies and Applications in Drug Design. *Chem. Rev.*
78            **2019**, *119*, 9478–9508, doi:10.1021/acs.chemrev.9b00055.

79    29.    Murray, C.W.; Erlanson, D.A.; Hopkins, A.L.; Keserü, G.M.; Leeson, P.D.; Rees, D.C.; Reynolds, C.H.;
80            Richmond, N.J. Validity of ligand efficiency metrics. *ACS Med. Chem. Lett.* **2014**, *5*, 616–618,
81            doi:10.1021/ml500146d.

82    30.    Hopkins, A.L.; Groom, C.R.; Alex, A. Ligand efficiency: a useful metric for lead selection. *Drug Discov.*
83            *Today* **2004**, *9*, 430–431, doi:10.1016/S1359-6446(04)03069-7.

84    31.    Abad-Zapatero, C. Ligand Efficiency Indices for Drug Discovery. *Ligand Effic. Indices Drug Discov.* **2013**,
85            *10*, 469–488, doi:10.1016/C2012-0-02270-3.

86    32.    Kenny, P.W. The nature of ligand efficiency. *J. Cheminform.* **2019**, *11*, 1–18, doi:10.1186/s13321-019-0330-
87            2.

88    33.    Xu, Y.; Yang, X.; Chen, Y.; Chen, H.; Sun, H.; Li, W.; Xie, Q.; Yu, L.; Shao, L. Discovery of novel 20S
89            proteasome inhibitors by rational topology-based scaffold hopping of bortezomib. *Bioorganic Med. Chem.*
90            *Lett.* **2018**, *28*, 2148–2152, doi:10.1016/j.bmcl.2018.05.018.

91    34.    Hopkins, A.L.; Keserü, G.M.; Leeson, P.D.; Rees, D.C.; Reynolds, C.H. The role of ligand efficiency
92            metrics in drug discovery. *Nat. Rev. Drug Discov.* **2014**, *13*, 105–121, doi:10.1038/nrd4163.

93    35.    Kauthale, S.; Tekale, S.; Damale, M.; Sangshetti, J.; Pawar, R. Synthesis, biological evaluation, molecular
94            docking, and ADMET studies of some isoxazole-based amides. *Med. Chem. Res.* **2018**, *27*, 429–441,
95            doi:10.1007/s00044-017-2070-z.

96    36.    Kumar, N.; Goel, N.; Chand Yadav, T.; Pruthi, V. Quantum chemical, ADMET and molecular docking
97           studies of ferulic acid amide derivatives with a novel anticancer drug target. *Med. Chem. Res.* **2017**, *26*,
98           1822–1834, doi:10.1007/s00044-017-1893-y.

99    37.    Tsaioun, K.; Blaauboer, B.J.; Hartung, T. Evidence-based absorption, distribution, metabolism, excretion
100          (ADME) and its interplay with alternative toxicity methods. *ALTEX* **2016**, *33*, 343–358,
101          doi:10.14573/altex.1610101.

102   38.    Teotia, P.; Prakash Dw, S.; Dwivedi, N. In silico Molecular Docking and ADME/Tox Study on
103          Benzoxazole Derivatives Against Inosine 5'-Monophosphate Dehydrogenase. *Asian J. Biotechnol.* **2018**,
104          *10*, 1–10, doi:10.3923/ajbkr.2018.1.10.

105   39.    Daina, A.; Michielin, O.; Zoete, V. SwissADME: a free web tool to evaluate pharmacokinetics, drug-
106          likeness and medicinal chemistry friendliness of small molecules. *Sci. Rep.* **2017**, *7*, 42717,
107          doi:10.1038/srep42717.

108   40.    Lipinski, C.A.; Lombardo, F.; Dominy, B.W.; Feeney, P.J. Experimental and computational approaches
109          to estimate solubility and permeability in drug discovery and development settings1PII of original
110          article: S0169-409X(96)00423-1. The article was originally published in Advanced Drug Delivery Reviews
111          23 (1997) 3–25.1. *Adv. Drug Deliv. Rev.* **2001**, *46*, 3–26, doi:https://doi.org/10.1016/S0169-409X(00)00129-0.

112   41.    Veber, D.F.; Johnson, S.R.; Cheng, H.-Y.; Smith, B.R.; Ward, K.W.; Kopple, K.D. Molecular Properties
113          That Influence the Oral Bioavailability of Drug Candidates. *J. Med. Chem.* **2002**, *45*, 2615–2623,
114          doi:10.1021/jm020017n.

115   42.    Hughes, J.D.; Blagg, J.; Price, D.A.; Bailey, S.; DeCrescenzo, G.A.; Devraj, R. V.; Ellsworth, E.; Fobian,
116          Y.M.; Gibbs, M.E.; Gilles, R.W.; et al. Physiochemical drug properties associated with in vivo
117          toxicological outcomes. *Bioorg. Med. Chem. Lett.* **2008**, *18*, 4872–4875, doi:10.1016/J.BMCL.2008.07.071.

118   43.    Hanwell, M.D.; Curtis, D.E.; Lonie, D.C.; Vandermeersch, T.; Zurek, E.; Hutchison, G.R. Avogadro: an
119          advanced semantic chemical editor, visualization, and analysis platform. *J. Cheminform.* **2012**, *4*, 17,
120          doi:10.1186/1758-2946-4-17.

121   44.    Neese, F. Software update: the ORCA program system, version 4.0. *Wiley Interdiscip. Rev. Comput. Mol.*
122          *Sci.* **2018**, *8*, e1327, doi:10.1002/wcms.1327.

123   45.    Neese, F. The ORCA program system. *Wiley Interdiscip. Rev. Comput. Mol. Sci.* **2012**, *2*, 73–78,
124          doi:10.1002/wcms.81.

125   46.    Morris, G.M.; Huey, R.; Lindstrom, W.; Sanner, M.F.; Belew, R.K.; Goodsell, D.S.; Olson, A.J. AutoDock4
126          and AutoDockTools4: Automated docking with selective receptor flexibility. *J. Comput. Chem.* **2009**, *30*,
127          2785–2791, doi:10.1002/jcc.21256.

128   47.   Berman, H.. M.; Westbrook, J.; Feng, Z.; Gilliland, G.; Bhat, T.N.; Weissig, H.; Shindyalov, I.N.; Bourne,
129          P.. E.; Westbrook, Z.; Feng, G.; et al. The Protein Data Bank. *Nucleic Acids Res.* **2000**, *28*, 235–242.

130   48.   Krimmer, S..; Klebe, G. Thermodynamics of protein-ligand interactions as a reference for computational
131          analysis: how to assess accuracy, reliability and relevance of experimental data. *J. Comput. Aided Mol.*
132          *Des.* **2015**, *29*, 867–883.

133   49.   Trott, O.; Olson, A.J. AutoDock Vina: improving the speed and accuracy of docking with a new scoring
134          function, efficient optimization, and multithreading. *J. Comput. Chem.* **2010**, *31*, 455–461,
135          doi:10.1002/jcc.21334.

136   50.   Koebel, M.R.; Schmadeke, G.; Posner, R.G.; Sirimulla, S. AutoDock VinaXB: implementation of XBSF,
137          new empirical halogen bond scoring function, into AutoDock Vina. *J. Cheminform.* **2016**, *8*, 27,
138          doi:10.1186/s13321-016-0139-1.

139   51.   Gohlke, H.; Hendlich, M.; Klebe, G. Knowledge-based scoring function to predict protein-ligand
140          interactions. *J. Mol. Biol.* **2000**, *295*, 337–56, doi:10.1006/jmbi.1999.3371.

141   52.   Velázquez-Libera, J.L.; Durán-Verdugo, F.; Valdés-Jiménez, A.; Núñez-Vivanco, G.; Caballero, J.
142          LigRMSD: a web server for automatic structure matching and RMSD calculations among identical and
143          similar compounds in protein-ligand docking. *Bioinformatics* **2020**, doi:10.1093/bioinformatics/btaa018.

144   53.   Schrödinger, LLC *The {PyMOL} Molecular Graphics System, Version~1.3r1*; 2010;

145   54.   Boonstra, S.; Onck, P.R.; Giessen, E. van der CHARMM TIP3P Water Model Suppresses Peptide Folding
146          by Solvating the Unfolded State. *J. Phys. Chem. B* **2016**, *120*, 3692–3698, doi:10.1021/acs.jpcb.6b01316.

147   55.   Lu, J.; Qiu, Y.; Baron, R.; Molinero, V. Coarse-Graining of TIP4P/2005, TIP4P-Ew, SPC/E, and TIP3P to
148          Monatomic Anisotropic Water Models Using Relative Entropy Minimization. *J. Chem. Theory Comput.*
149          **2014**, *10*, 4104–4120, doi:10.1021/ct500487h.

150   56.   Vincent, Z.; A., C.M.; Aurélien, G.; Olivier, M. SwissParam: A fast force field generation tool for small
151          organic molecules. *J. Comput. Chem. 32*, 2359–2368, doi:10.1002/jcc.21816.

152   57.   Lee, J.; Cheng, X.; Swails, J.M.; Yeom, M.S.; Eastman, P.K.; Lemkul, J.A.; Wei, S.; Buckner, J.; Jeong, J.C.;
153          Qi, Y.; et al. CHARMM-GUI Input Generator for NAMD, GROMACS, AMBER, OpenMM, and
154          CHARMM/OpenMM Simulations Using the CHARMM36 Additive Force Field. *J. Chem. Theory Comput.*
155          **2016**, *12*, 405–413, doi:10.1021/acs.jctc.5b00935.

156   58.   Mackerell, A.D.; Feig, M.; Brooks, C.L. Extending the treatment of backbone energetics in protein force
157          fields: limitations of gas-phase quantum mechanics in reproducing protein conformational distributions
158          in molecular dynamics simulations. *J. Comput. Chem.* **2004**, *25*, 1400–15, doi:10.1002/jcc.20065.

59.  Soteras Gutiérrez, I.; Lin, F.-Y.; Vanommeslaeghe, K.; Lemkul, J.A.; Armacost, K.A.; Brooks, C.L.; MacKerell, A.D. Parametrization of halogen bonds in the CHARMM general force field: Improved treatment of ligand–protein interactions. *Bioorg. Med. Chem.* **2016**, *24*, 4812–4825, doi:10.1016/j.bmc.2016.06.034.

60.  Vanommeslaeghe, K.; Hatcher, E.; Acharya, C.; Kundu, S.; Zhong, S.; Shim, J.; Darian, E.; Guvench, O.; Lopes, P.; Vorobyov, I.; et al. CHARMM general force field: A force field for drug-like molecules compatible with the CHARMM all-atom additive biological force fields. *J. Comput. Chem.* **2010**, *31*, 671–690, doi:10.1002/jcc.21367.

61.  Vanommeslaeghe, K.; Yang, M.; MacKerell, A.D. Robustness in the fitting of molecular mechanics parameters. *J. Comput. Chem.* **2015**, *36*, 1083–1101, doi:10.1002/jcc.23897.

62.  Berendsen, H.J.C.; Postma, J.P.M.; Gunsteren, W.F. Van; Nola, A. Di; Haak, J.K. Molecular Dynamics with coupling to an external bath. *J. Chem. Physic* **1984**, *81*, 3684–3690.

63.  Onufriev, A.; Bashford, D.; Case, D.A. Exploring protein native states and large-scale conformational changes with a modified generalized born model. *Proteins Struct. Funct. Bioinforma.* **2004**, *55*, 383–394, doi:10.1002/prot.20033.

64.  Phillips, J.C.; Braun, R.; Wang, W.; Gumbart, J.; Tajkhorshid, E.; Villa, E.; Chipot, C.; Skeel, R.D.; Kalé, L.; Schulten, K. Scalable molecular dynamics with NAMD. *J. Comput. Chem.* **2005**, *26*, 1781–802, doi:10.1002/jcc.20289.

65.  Dalke, W.; Humphrey, A.; Schulten, K. VMD - Visual Molecular Dynamics. *J. Mol. Graph.* **1996**, *14*, 33–38.

66.  Kumari, R.; Kumar, R.; Lynn, A. G-mmpbsa -A GROMACS tool for high-throughput MM-PBSA calculations. *J. Chem. Inf. Model.* **2014**, *54*, 1951–1962, doi:10.1021/ci500020m.

67.  Baker, N.A.; Sept, D.; Joseph, S.; Holst, M.J.; McCammon, J.A. Electrostatics of nanosystems: Application to microtubules and the ribosome. *Proc. Natl. Acad. Sci. U. S. A.* **2001**, *98*, 10037–10041, doi:10.1073/pnas.181342398.

68.  Abad-Zapatero, C.; Perišić, O.; Wass, J.; Bento, A.P.; Overington, J.; Al-Lazikani, B.; Johnson, M.E. Ligand efficiency indices for an effective mapping of chemico-biological space: The concept of an atlas-like representation. *Drug Discov. Today* **2010**, *15*, 804–811, doi:10.1016/j.drudis.2010.08.004.

69.  Meneses, L.; Cuesta, S. Determinación Computacional de la Afinidad y Eficiencia de Enlace de Antinflamatorios No Esteroideos Inhibidores de la Ciclooxigenasa-2. *Rev. Ecuat. Med. Cienc. Biol.* **2017**, *36*, 17, doi:10.26807/remcb.v36i1-2.260.

190   70.   Reynolds, C.H.; Tounge, B.A.; Bembenek, S.D. Ligand Binding Efficiency: Trends, Physical Basis, and
191         Implications. *J. Med. Chem.* **2008**, *51*, 2432–2438, doi:10.1021/jm701255b.

192   71.   Kenny, P.W.; Leitão, A.; Montanari, C.A. Ligand efficiency metrics considered harmful. *J. Comput. Aided.*
193         *Mol. Des.* 2014, *28*, 699–710.

194   72.   Polanski, J.; Tkocz, A.; Kucia, U. Beware of ligand efficiency (LE): Understanding LE data in modeling
195         structure-activity and structure-economy relationships. *J. Cheminform.* **2017**, *9*, 49, doi:10.1186/s13321-
196         017-0236-9.

197   73.   Hopkins, A.L.; Keserü, G.M.; Leeson, P.D.; Rees, D.C.; Reynolds, C.H. The role of ligand efficiency
198         metrics in drug discovery. *Nat. Rev. Drug Discov.* **2014**, *13*, 105–121, doi:10.1038/nrd4163.

199   74.    Duchowics, P.R.; Talevi, A.; Bellera, C.; Bruno-Blanch, L.E.; Castro, E.A.; Duchowicz, P.R.; Talevi, A.;
200   Bellera, C.; Bruno-Blanch, L.E.; Castro, E.A. Application of descriptors based on Lipinski's rules in the QSPR
201   study of aqueous solubilities. *Bioorg. Med. Chem.* **2007**, *15*, 3711–3719, doi:10.1016/j.bmc.2007.03.044.
202